Solar Physics (2006) 239: 277–292
DOI: 10.1007/s11207-006-0202-6

A RADIO BURST AND ITS ASSOCIATED CME ON MARCH 17, 2002

Y. YAN
National Astronomical Observatories, Chinese Academy of Sciences, Beijing 100012, P.R. China (e-mail: yyh@bao.ac.cn)

M. PICK
LESIA, UMR 8109 CNRS, Observatoire de Paris/Meudon, 92195 Meudon, France

M. WANG
National Astronomical Observatories, Yunnan Observatory, Chinese Academy of Sciences, Kunming 650011, P.R. China

S. KRUCKER
Space Research Laboratory, University of California, 7 Gauss Way, Berkeley, CA 94720-7450, U.S.A.

and

A. VOURLIDAS
Naval Research Laboratory, Code 7660, NRL 4555, Overlook Avenue, SW, Washington, DC 20375, U.S.A.

(Received 13 April 2006; accepted 2 October 2006; Published online 26 November 2006)

Abstract. In this study, we present a detailed analysis, based on multiwavelength observations and magnetic field extrapolation, of a radio and X-ray event observed on March 17, 2002. This event was accompanied by a Coronal Mass Ejection (CME) observed by the Large-Angle Spectrometric Coronagraph (LASCO) aboard SOHO. During the main event, the Reuven Ramaty High-Energy Solar Spectroscopic Imager (RHESSI) mission observed a hard X-ray emission correlated in time with the development of a type III burst group. The CME development, the hard X-ray emission, and the type III burst group appear to be closely associated. The multifrequency Nançay Radioheliograph (NRH) shows that the type III bursts are produced at a distance from the active region that progressively increases with time. Their emitting sources are distributed along the western edge of the CME. We conclude the type III electron beams propagate in the interface region between the ascending CME and the neighboring open field lines. Due to the development of the CME, this region becomes progressively highly compressed. By measuring, at each frequency, the shift versus time of the type III positions, we estimate that the electron density in this compression region increased roughly by a factor of 10 over a few minutes. Another signature of this compression region is a narrow white light feature interpreted as a coronal shock driven by the CME lateral expansion.

1. Introduction

Since their discovery by Tousey (1973), Coronal Mass Ejections (CMEs) have been observed by numerous white light coronagraphs. Comparison of the CME observations from the SOHO (Solar and Heliospheric Observatory) instruments with

complementary coronal observations made it possible to follow the progression of CMEs and related phenomena from the low corona to the interplanetary medium. CMEs are associated with on-disk manifestations that have been observed in EUV, soft X-rays, and radio. The main advantages of coronal radio observations over other wavelengths are the high cadence (<1 second); they enable detailed analysis of the initiation and early development of CMEs, in particular, when the period of acceleration is short, specifically 10 minutes or shorter. Radio observations are sensitive to different aspects of CMEs, depending on the selected observing wavelength domain. CMEs are frequently accompanied by flares and the current view is that these events are two different manifestations of a common magnetic energy release. Both flares and CMEs can be associated with particle acceleration. Energetic electrons that are detected in the corona by their observed X-ray and radio signatures, originate in shocks or in regions of magnetic interaction between loop systems participating in the eruption process. Type II bursts are believed to be the signature of coronal shocks. Type III bursts are generated by electron beams, with energy of the order of a few tens of keV, which propagate along open magnetic field lines. Radio continua reveal populations of suprathermal to MeV electrons injected into expanding arches or posteruptive loops behind the CME leading edges. To understand the development of CMEs and their link with electron acceleration, it is very important to test which magnetic flux systems participate in the eruption and how energetic electrons propagate in the corona and then in the interplanetary medium. This can only be done using magnetic field extrapolation to infer the preeruptive topology.

In this study, we present a detailed analysis, based on multiwavelength observations and magnetic field extrapolation, of a radio and X-ray event observed on March 17, 2002. This event was associated with a CME observed by the Large-Angle Spectrometric Coronagraph (LASCO; Brueckner *et al.*, 1995). A M1.3 GOES flare (starting at 10:11 UT, peaking at 10:19 UT, and ending at 10:24 UT) was reported by *Solar Geophysical Data* (`http://www.ngdc.noaa.gov/stp`). There were no Hα patrol observations around this time. The RHESSI mission (Lin *et al.*, 2002) observed a hard X-ray emission above the complex active region 9871 at S20E24 location.

The sources of radio data were the images at five frequencies (164, 236.6, 327, 410, and 432 MHz) of the Nançay Radioheliograph (NRH) (Kerdraon and Delouis, 1997) and dynamic spectra from different radio spectrographs: the Tremsdorf spectrometer (OSRA) from 40 to 800 MHz (available in the present study below 400 MHz) (Mann *et al.*, 1992), the Nançay Decameter Array (DAM) from 20 to 70 MHz (Lecacheux, 2000) and WIND/WAVES from 20 kHz to 14 MHz (Bougeret *et al.*, 1995). For the magnetic extrapolation, we used photospheric magnetograms obtained from the Michelson Doppler Imager (MDI/SOHO) (Scherrer *et al.*, 1995).

The data analysis is presented in Section 2. We then determine in Section 3 the coronal magnetic field line topology in the vicinity of AR 9871 by applying a potential field extrapolation. From the results of this extrapolation, we can identify

the key structures in which energetic electrons are injected and propagate. Discussions and conclusions are given in Section 4.

2. Data Analysis

2.1. X-RAY AND RADIO OBSERVATIONS

Figure 1 shows a comparison between the photon history measured by RHESSI in the 30 – 100 keV energy range and the radio spectral evolution measured by OSRA and WAVES. A first group of type III bursts is detected at 10:08 UT at frequencies higher than 100 MHz. The main event, observed after 10:12 UT, coincides with the strong hard X-ray increase. Radio emission in the metric wavelength range and the X-ray emission are strongly coupled. The radio event is composed of a series of

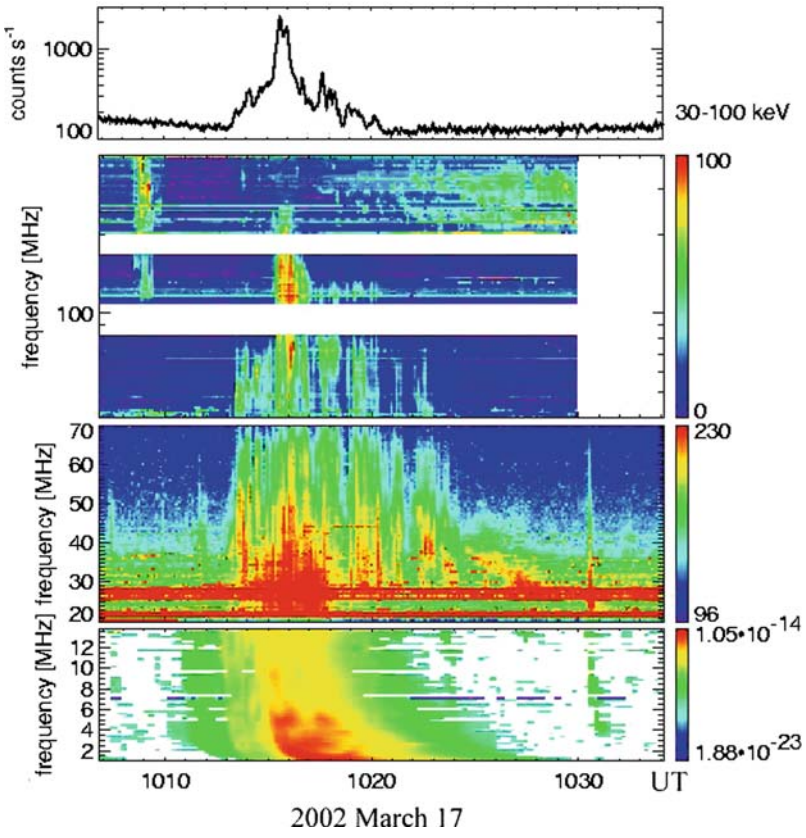

Figure 1. Time history of the March 17, 2002 event: *Top panel* shows the 30 – 100 keV hard X-ray time profile detected by RHESSI; *below* radio spectrograms observed by OSRA, DAM, and WIND/WAVES are shown.

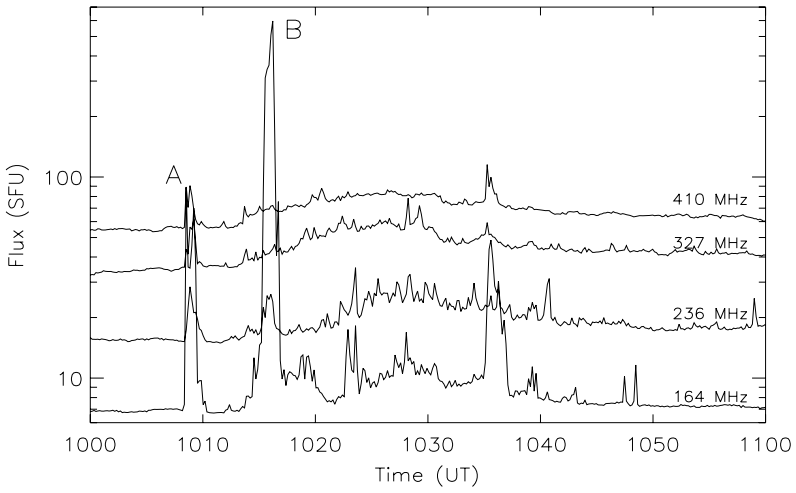

Figure 2. Global flux history of the radio burst on March 17, 2002.

fast drifting type III bursts, with a drift rate of the order of 300 MHz s^{-1}. Figure 2 displays the flux evolution measured at four frequencies by the NRH versus time. Following the two groups of type III bursts, labeled A and B in this figure, the onset of a broad frequency continuum is detected at all the NRH frequencies. The flux of this continuum increases progressively, then more rapidly after burst B.

We shall focus in the following subsections on the data analysis of events A, B and of the continuum.

2.1.1. *Event A*

Figure 3 shows the positions of the emitting sources measured at four frequencies with a cadence of 1 second superposed on an Hα image. At 236 MHz, there were two emitting regions around AR 9871, one to the east and one to the west. The positions measured at 164 MHz, above the active region, spread between these two regions. At higher frequencies, only the western region is detected. The type III bursts are not detected below 100 MHz. These imaging and spectral observations suggest that most of the electron beams generating the radio emission propagated in closed coronal loops, consistent with the reconstructed magnetic configuration as will be demonstrated in Section 3.2. We also note that the western source is more bursty than the eastern source when observing the evolution of their intensity measured at 236 MHz and at a cadence of 1 second. These observations suggest that most of type III bursts have their origin near the western edge of AR 9871. At 164 MHz, a few other burst positions are also detected south-west from the active region.

2.1.2. *Event B*

Figure 4 shows the contour plots at 10:15 UT of the hard and soft X-ray sources superposed on an MDI map of the magnetic field.

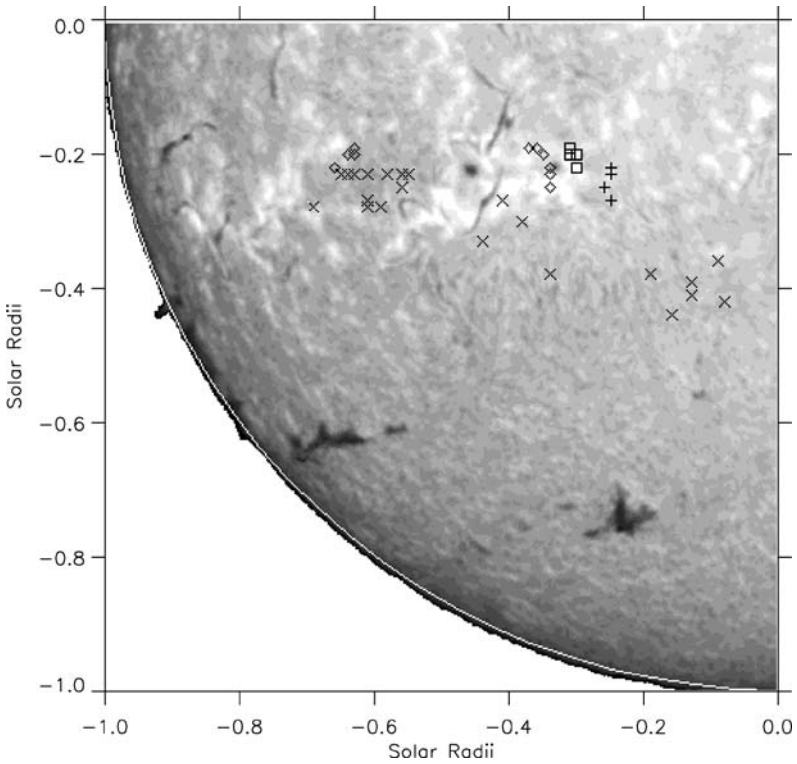

Figure 3. Radio sources of Event A (see Figure 2) at the four NRH frequencies superposed on a Hα image, which does not correspond to the flare time (no Hα patrol available at this time). The symbols: *cross, diamond, square*, and *plus* represent the sources at 164, 236, 327, and 410 MHz, respectively.

The hard X-ray source includes three components. The west one is located above a positive polarity surrounding the negative leading polarity of AR 9871, while the middle and the east ones are located above areas with negative and positive polarities mixed. The SXR contours appear to outline two adjacent loops with the three HXR sources located at their footpoints.

Figure 5 shows an Hα image of the day on which the locations of the RHESSI source and of the emitting radio sources measured at all the NRH frequencies are reported. In radio, the same eastern region as for event A is detected, but exclusively at frequencies higher than 164 MHz; type III bursts are now observed at all NRH frequencies above the western region, during the period 10:13 – 10:17 UT (the bursts are detected until 10:21 UT at 164 MHz). The positions versus time of the type III emitting sources, measured at 236 and 164 MHz with a cadence of 1 second, are reported in Figure 6. Figures 5 and 6, considered together, show that the locations of these bursts shift progressively toward the south with a projected displacement of 600 km s^{-1}. A weak shift toward the west is also seen at each single frequency.

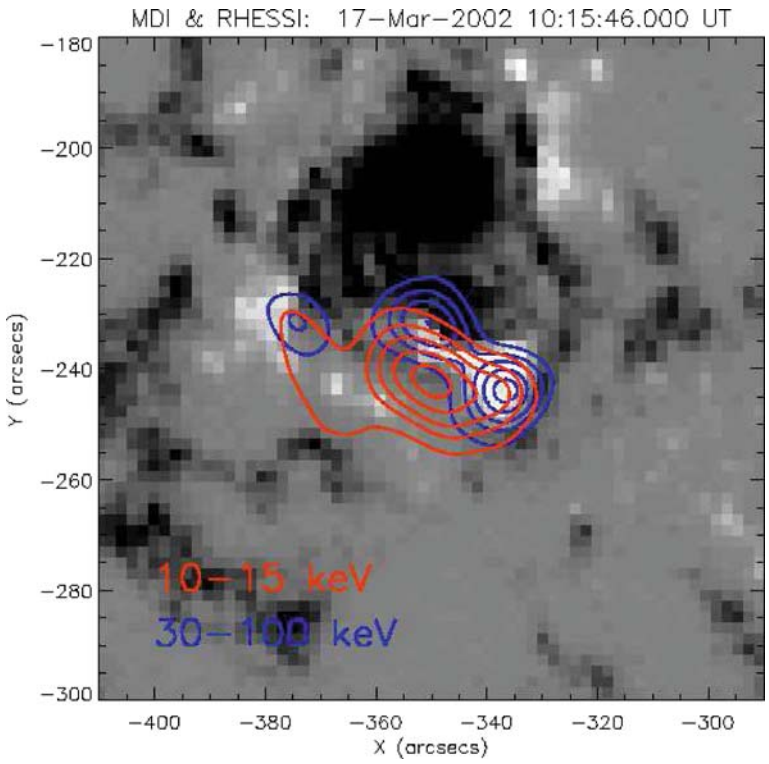

Figure 4. X-ray imaging from RHESSI (CLEANed images with a spatial resolution of 10 arcseconds) of event B (see Figure 2). Thermal (10 – 15 keV, *red*) and nonthermal (30 – 100 keV, *blue*) X-ray contours are superposed on an MDI magnetogram. The shown contours are 20, 35, 50, 70, and 90% of the maximum emission.

2.1.3. *Continuum Emission*

Figure 2 shows that the long duration continuum appears progressively after 10:10 UT. This continuum originates near AR 9871 in the eastern side and shifts progressively toward the north, from 0.35 $R_{\odot}$ South to 0.1 $R_{\odot}$ North at 164 MHz. The positions, which are reported in Figure 7, roughly coincide at all frequencies measured by the NRH.

2.2. THE CORONAL MASS EJECTION

Figure 8 shows two successive LASCO images of the CME development in the C2 field of view. The CME has the appearance of a bright loop in expansion that propagates in the southward direction. In addition, a narrow structure becomes visible in the image at 10:56 UT (see label *I*, which is still faintly present in the next C2 image at 11:06 UT) and propagates transversally to the direction of the

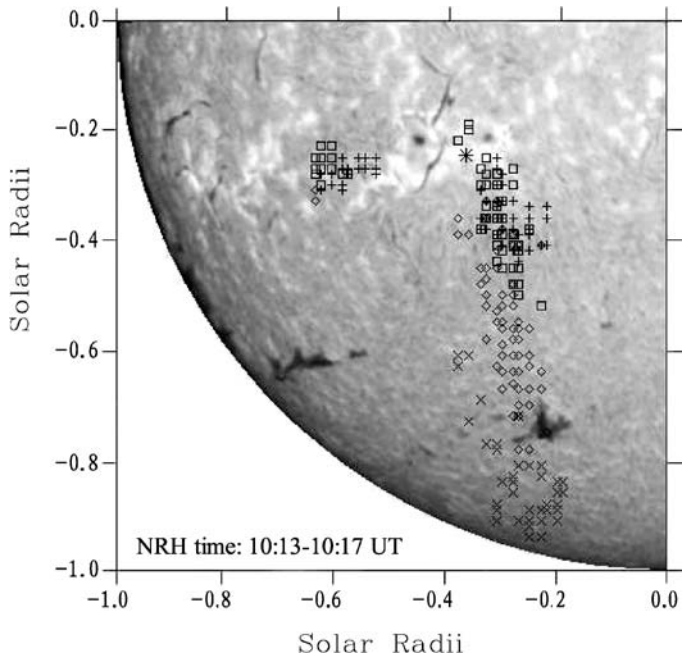

Figure 5. Event B: Radio sources at the four NRH frequencies superposed on the same Hα image as in Figure 3. The symbols, *cross, diamond, square*, and *plus* represent the sources of 164, 236, 327, and 410 MHz, respectively. The *star* symbol represents schematically the position of the corresponding hard X-ray source.

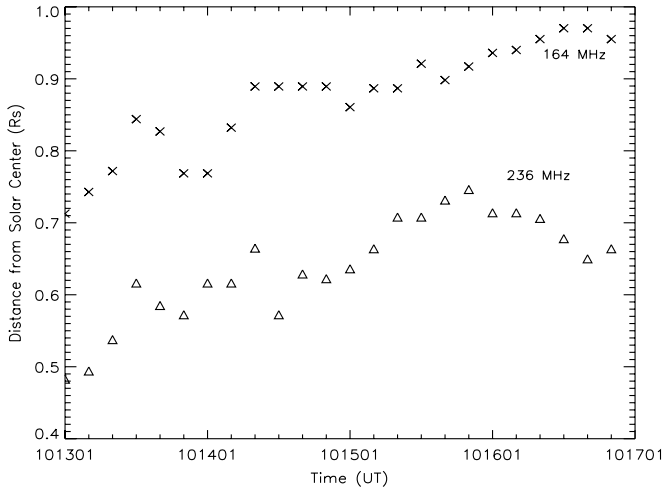

Figure 6. Event B: Shift versus time of the type III radio sources measured at 164 and 236 MHz.

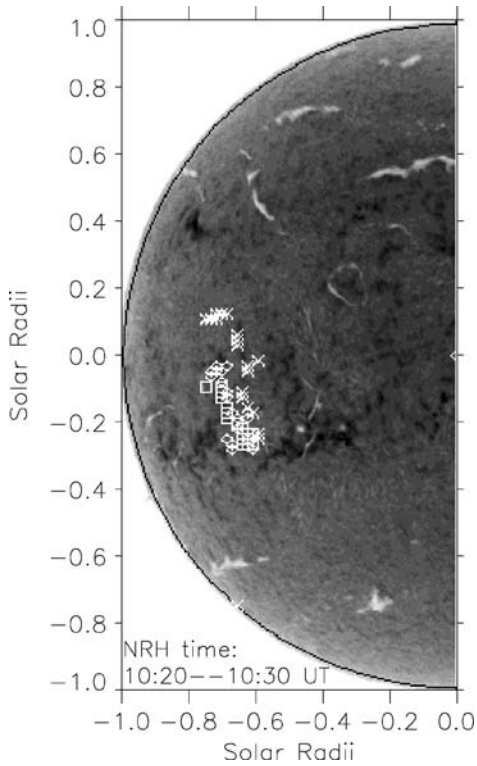

Figure 7. Positions of the radio continuum (see Figure 2) measured at the four NRH frequencies and superposed on the same Hα image as in Figures 3 and 5. The symbols, *cross, diamond, square*, and *plus* represent the sources of 164, 236, 327, and 410 MHz, respectively.

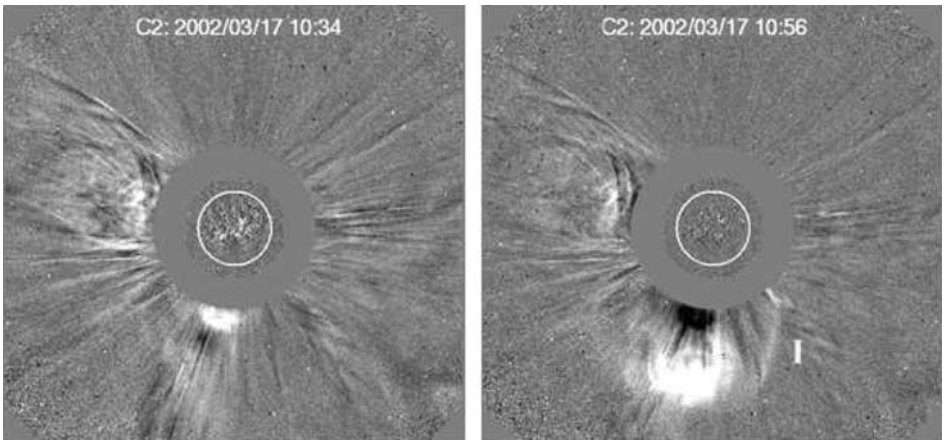

Figure 8. Two LASCO C2 images showing the development of the CME in the south hemisphere. The structure labeled *I* is interpreted as the signature of a coronal shock (see text).

CME propagation. The narrow ray visible at the base of this structure is brighter at 10:56 UT than at 10:34 UT and could be the signature of a compression. The morphology of this structure is consistent with the signatures of a coronal shock propagating away from the western edge of the CME; this shock is probably associated with the type II burst starting around 10:24 UT and visible below 40 MHz in Figure 1. In the C3 image of 11:18 UT, the front of the CME was seen at the height of 7.56 $R_{\odot}$. The height–time curves (second-order fit) shows that the projected velocity of this CME is about 900 km s^{-1} and decelerates with a rate of the order of 31 km s^{-1}.

2.3. Summary of the data analysis

We have made a detailed data analysis of the March 17, 2002 event. Any interpretation of this event must be consistent with the following characteristics:

- At first, radio burst A develops above the active region. The locations of the radio sources measured at various frequencies provide evidence for electrons injected in coronal loops generating continuum emission near the eastern feet of these loops.
- A second major radio event B composed predominantly of a group of type III bursts lasting for several minutes and associated with the development of a CME. The type III emitting sources are approximately distributed along the inward direction of the western edge of the CME. These sources shift outward with a projected displacement of 600 km s^{-1}. A weak shift toward the west is also seen at each single frequency.
- A close spatial and temporal association is observed between the hard X-ray and radio emissions during event B. The HXR source is composed of three components located at the footpoints of two adjacent SXR sources.
- A subsequent radio continuum develops near the eastern edge of the active region. The source moves progressively from south to north over a distance of about 0.45 $R_{\odot}$.
- A narrow white light structure is seen in the LASCO images at 10:56 UT, interpreted as the signature of a coronal shock that propagates transverse to the direction of the CME. This is consistent with the detection of a type II-like feature below 40 MHz observed at about 10:24 UT.

3. Coronal Field Reconstruction

3.1. Brief description of the potential model

We have seen in the previous sections that the spatial and temporal distribution of the radio sources are complex. In order to understand the physical process involved

in this event, we reconstructed the 3-D magnetic structure. The extrapolation is based on a potential magnetic code (e.g., Yan, Yu, and Shi, 1993; and recently in Wang *et al.*, 2002; Yan, 2005). Under the potential condition ($\nabla \times \mathbf{B} = 0$), the magnetic field can be represented by a scalar potential Ψ with $\mathbf{B} = -\nabla \Psi$ and $\nabla^2 \Psi = 0$. On the solar surface S, we have $B_n = -\partial \Psi / \partial n$ which are specified. In general, the potential Ψ at any position $\mathbf{r}_i$ in space V can be determined from Green's Second Identity (Courant and Hilbert, 1962). The magnetic field can then be obtained with $\partial \Psi / \partial n$ known over the boundary and Ψ solved numerically by the boundary element method (Yan, Yu, and Shi, 1993).

We have employed MDI/SOHO daily synoptic magnetograms to obtain the boundary conditions over the whole solar surface. Due to the projection effect, we employed MDI magnetogram data in the central region of $\pm 50^\circ$ longitude and $\pm 50^\circ$ latitude and the MDI daily synoptic magnetogram data in the regions of -180° to -50° and $50 - 180^\circ$ longitude, and $\pm 60^\circ$ latitude.

3.2. Reconstructed magnetic field structures

From the results of this extrapolation, we can analyze the topology of the magnetic field prior to the onset of the March 17, 2002 event.

Figure 9 shows the MDI magnetogram overlaid by magnetic field lines calculated from the potential field extrapolation for the region where the radio sources of event A (10:08 – 10:11 UT) are detected. The sites of these sources are also reported on the same figure. We note that most of these sources are located along the large east–west loop system (green color). A few sources of type III bursts measured at 164 MHz are detected along open field lines (red color).

Figure 10 shows, for event B, the location of the hard X-ray and radio sources superposed on the same magnetic field configuration as for Figure 9. The hard X-ray sources appear to be located in a region where both the loop system and open field lines are rooted. However, this global field reconstruction does not reproduce the two small SXR loops. The eastern radio emitting region is the same as in Figure 9. The positions of the type III bursts are all located along open field lines rooted near the western edge of AR 9871. The sources of these type III bursts, measured at 164 and 236 MHz, move progressively toward the south-west direction. The reconstructed global magnetic field lines inserted in the LASCO/C2 image at 10:34 UT are shown in Figure 11. In this figure, the red lines indicate open field lines and blue (green in the previous figures) ones indicate closed lines. The type III radio source locations detected during event B are also reported in this figure. These radio sources are located approximately along and around the west edge of the CME.

Figure 12 shows the magnetic field extrapolation for the region, where the emitting sources of the continuum are detected (10:20 – 10:30 UT). These sources appear to progressively shift toward the north along an east–west arch system covering a large range of latitude.

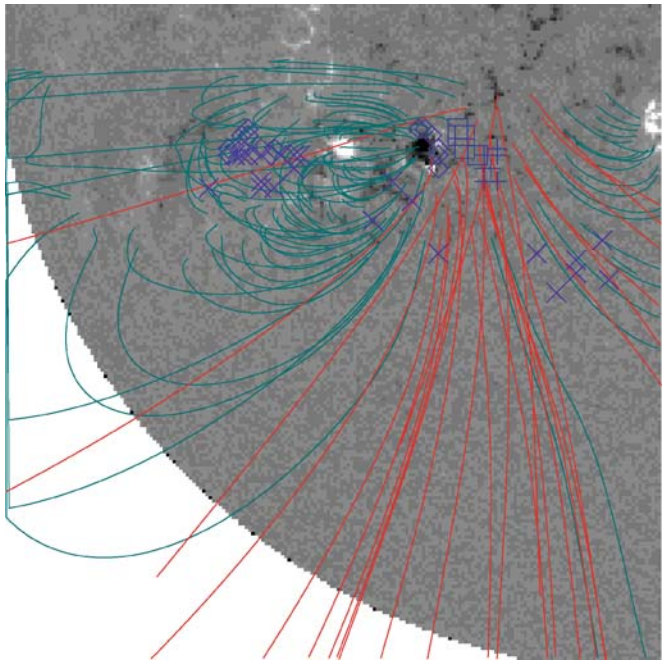

Figure 9. The radio sources for Event A shown in Figure 3 are superposed on the MDI magnetogram with the reconstructed magnetic field structure represented by open (*red*) and closed (*green*) field lines.

4. Discussion and Conclusions

The calculated topology allows us to suggest an interpretation of our results listed in Sections 2 and 3.

The CME developed above the large extrapolated southern loops (see Figure 10) that are adjacent to the open field lines.

The March 17, 2002 event occurred in a complex multipolar configuration of the magnetic field resulting from the location of AR9871 inside an old remnant region and from the local inclusion of small interacting loops around the leading negative polarity of this AR (see Figure 4). The small interacting loops can be inferred from SXR/HXR observations as represented in Figure 10, right panel. The west HXR component is cospatial with a positive magnetic polarity surrounding the negative leading polarity and negative open field lines. However the middle and east HXR components are located above both negative and positive polarities. The positive polarity of the east HXR component is connected to a loop further eastward; therefore, the two small loops by which each of them join an eastern negative polarity to a western positive polarity, form a "VV-shaped" structure. Note that the intensity of the leading SXR loop is higher than that of the other one

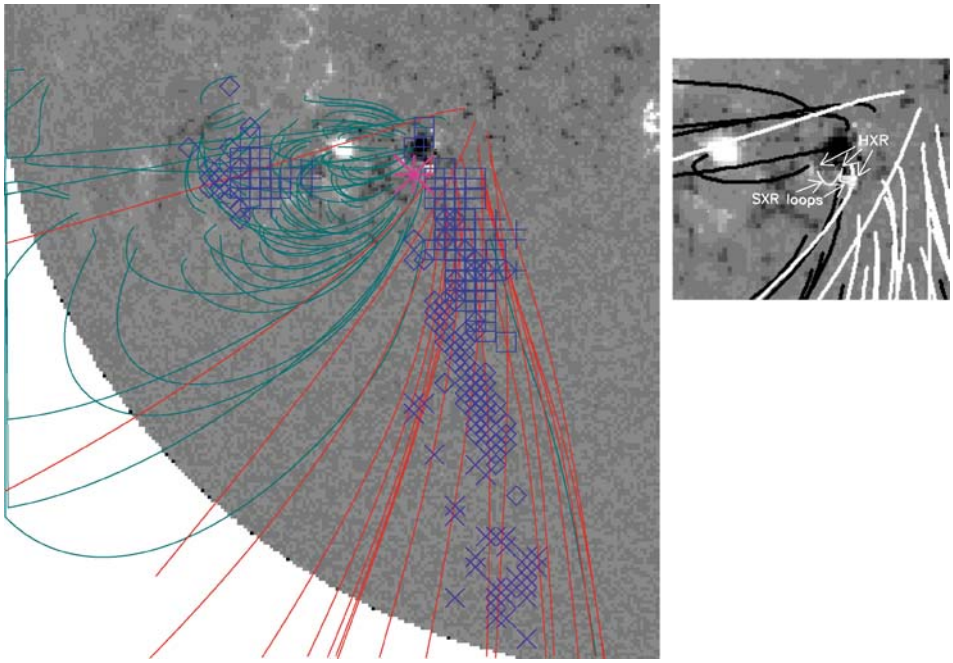

Figure 10. The radio sources for Event B shown in Figure 5 are superposed on the MDI magnetogram with the reconstructed magnetic field structure represented by open (*red*) and closed (*green*) field lines. The *pink "star"* symbol indicates the RHESSI HXR location. The *right panel* shows schematically the locations of the three HXR components and of the two SXR loops in the reconstructed magnetic field environment.

(Figure 4). The three HXR sources seen in Figure 4 overlie the three footpoints of the "VV-shaped" structure.

This topology of the magnetic field strongly suggests the existence of coronal null points near the local positive polarities. Magnetic reconnection can occur at these null points and thus will give rise to accelerated electrons that produce the radio emission detected during event A. This radio burst develops above the complex closed-and-open loop system. Presumably, electrons are injected near the interfaces of closed-and-open coronal loops and are confined in the closed coronal loops, generating continuum emission near the eastern feet of these loops. The western sources are located along the open field lines, generating type III bursts.

During event B, the CME, the hard X-ray emission, and the group of type III bursts seem to be coupled; there is a close temporal relationship between the hard X-ray and type III emissions. Sprangle and Vlahos (1983) proposed that electromagnetic radiation excited by an unstable electron velocity distribution inside a flaring loop may escape the loop and accelerate electrons along an open flux tube. In this interpretation, the hard X-ray produced inside the flaring loop and the type III bursts have a common energy source: the precipitating electrons. This scenario,

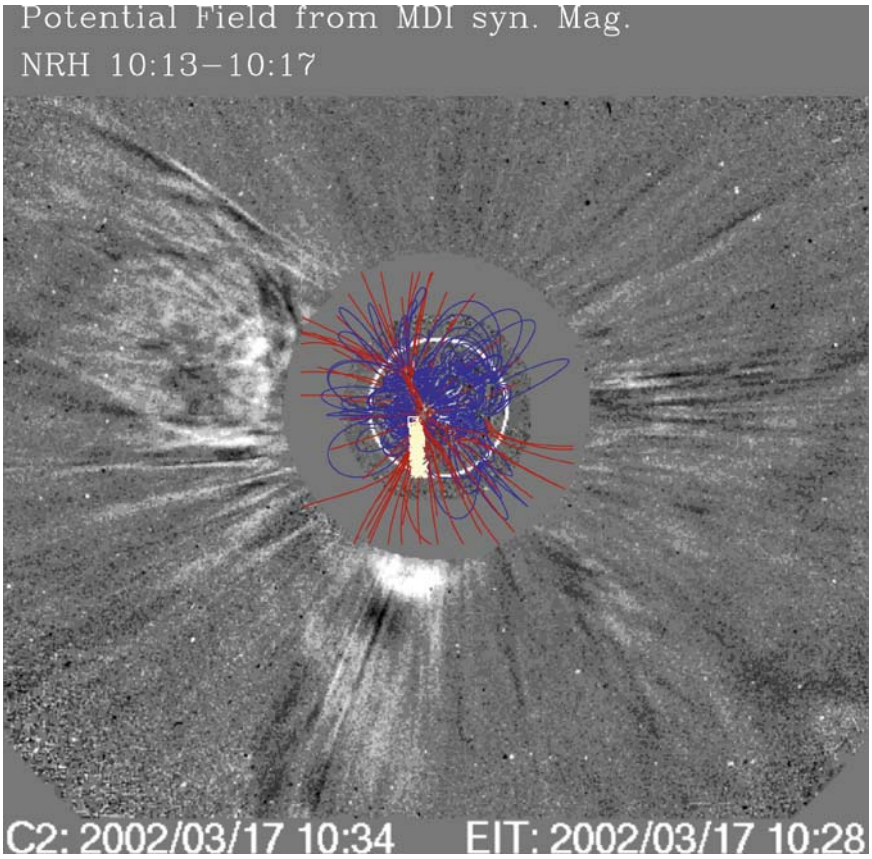

Figure 11. The reconstructed global magnetic field lines superposed on the LASCO/C2 image at 10:34. The *red* lines indicate open field lines and *blue* ones indicate closed field lines. The type III radio sources measured during event B at the four NRH frequencies (with the same symbols as in Figure 10) are plotted in *white*.

which was simulated for a static magnetic field bipolar configuration, can be easily extended to dynamical conditions. In a rising loop, the emitting regions for electrons will move up and escaping electrons will generate type III bursts. The March 17, 2002 event probably had poor magnetic connections to ACE and thus no interplanetary energetic electron event was detected.

We suggest, however, that the radio and X-ray emissions are produced by the same population of accelerated electrons. Similar to event A, the accelerated electrons will result from magnetic field interaction. The region, which is the site of the X-ray emission, is composed of two small loops that emerge inside or close to a large open unipolar region. One of them (or the two loops after interaction with each other) will interact with the surrounding open field lines and will generate accelerated electrons. The hard X-ray emission will be produced by electrons

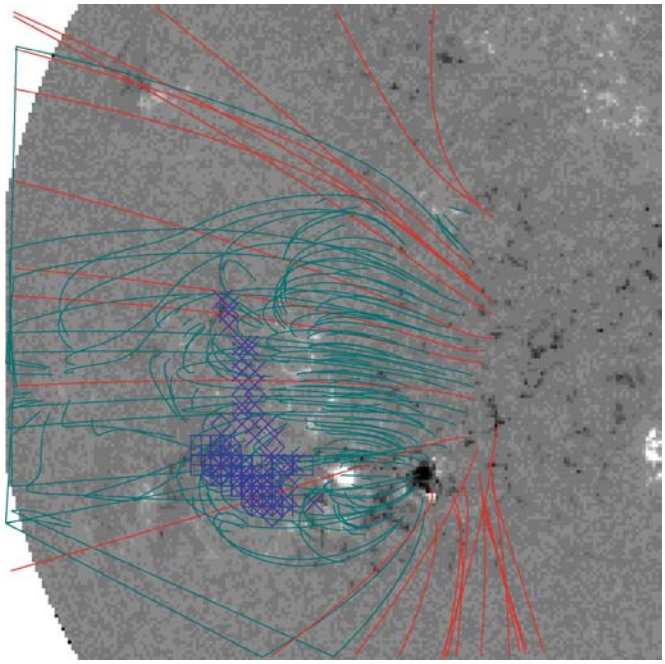

Figure 12. The radio sources for continuum emission shown in Figure 6 are superposed on the MDI magnetogram with the reconstructed magnetic field structure represented by open (*red*) and closed (*green*) field lines.

propagating downward, whereas outward electron beams, producing type III bursts, will propagate in the interface region between the ascending CME and the neighboring open field lines. Due to the development of the CME, this region becomes progressively highly compressed. The density that increases due to this compression process may be evaluated under the assumption of plasma emission at the second harmonic plasma frequency. The calculated open field lines have a projection angle of about 65°. If we consider that the type III bursts are produced along these open lines, we can estimate, for each frequency, the starting and ending altitudes: $R_s = R_\odot + | D_{Ls}\text{-}D_{Lf}| /\cos 65^\circ$, where R_s and D_{Ls} are the radial distance and the latitude of the emitting source, respectively; D_{Lf} is the solar latitude of the footpoint.

Therefore, the apparent motions of type III bursts at 410, 327, 236, and 164 MHz start at 10:13 UT at 1.07, 1.07, 1.38, and 1.92 solar radius, respectively, and end at 10:16 UT at 1.52, 1.59, 2.14, and 2.70 solar radius, respectively. By the Newkirk (1961) Model, the estimated density increases for frequencies higher than 164 MHz are about 10 times during event B, whereas the density increase at 164 MHz is about four times during the same period. At this frequency, a larger region is covered by the emitting sources and might account for this smaller density increase.

The radio type II burst detected after 10:22 UT, 10 minutes later than the onset of type III bursts, should not be at the origin of the electron acceleration producing type III bursts. This type II burst is associated with the shock detected later on in white light. In the present case, it seems difficult to explain the hard X-ray source (and the close correlation between the HXR emission and the type III bursts) with a driven-shock acceleration model. Indeed: (i) It takes time for a driven disturbance to steepen into a shock. The appearance of the type II about 10 minutes after the impulsive phase of the flare is consistent with that and consistent with our interpretation of a compression at the flank of the CME. Furthermore, we did not find evidence for reverse drift bursts at decimeter, metric, and decameter wavelengths. Therefore, it is highly unlikely that there existed a CME-driven shock during the type III and HXR emissions. (ii) The type-IIIs disappear almost as soon as the HXR sources fade and approximately when the radio shock signature appears in the DAM spectrum.

Finally, the continuum that progressively shifts toward the north along an east–west arch system may be attributed to accelerated electrons injected into arches from the vicinity of the flare site when posteruptive loops are formed.

In conclusion, by using a multiwavelength approach, we were able to study the early development of a CME. We give evidence, particularly for what we think to be the build-up of the compression region located between closed and open field lines. The radio signature of this region is the production of decimetric–metric type III bursts; the progressive shift versus time of their emitting sources is interpreted as an increase of the local plasma frequency, thus of the electron density. A similar signature was observed during the October 28, 2003 event (Pick *et al.*, 2005). Another signature of this compression region is the narrow white light feature interpreted as a coronal shock driven by the CME lateral expansion.

Acknowledgements

We are grateful to Loukas Vlahos and S. White for helpful discussions. The use of online data from SOHO/LASCO and other databases is acknowledged. YY and WM are supported by MOST (G2000078403, 2006CB806301, 2006CB806303) and NSFC (Nos. 10225313, 10333030, and 10473020) Grants. WM is also supported by the Project of Cultivating Western Talents of CAS. The visits of YY and WM to Meudon were supported under CAS–CRNS programs. The authors thank the SOHO LASCO and MDI consortia for their data. SOHO is a joint project by ESA and NASA. They also thank the RHESSI consortium for their data. Finally, they thank the anonymous referee for the helpful comments, which helped improve this paper; and they thank the editor, Lidia van Driel-Gesztelyi, for helpful editorial work.

References

Bougeret, J.-L., Kaiser, M.L., Kellogg, P.J., Manning, R., Goetz, K., Monson, S.J., *et al.*: 1995, *Space Sci. Rev.* **71**, 231.

Brueckner, G.E., Howard, R.A., Koomen, M.J., Korendyke, C.M., Michels, D.J., Moses, J.D., Socker, D.G. *et al.*: 1995, *Solar Phys.* **162**, 357.

Courant, R. and Hilbert, D.: 1962, *Methods of Mathematical Physics*, Vol. II, Interscience, New York.

Kerdraon, A. and Delouis, J.M.: 1997, in G. Trottet (ed.), *Coronal Physics from Radio and Space Observation*, Lecture Notes in Physics, Vol. 483, Springer-Verlag, Berlin, p. 192.

Lecacheux, A.: 2000, in R.G. Stone (ed.), *Radio Astronomy at Long Wavelengths*, AGU, Washington, DC, p. 321.

Lin, R.P., Dennis, B.R., Hurford, G.J., Smith, D.M., Zehnder, A., Harvey, P.R., *et al.*: 2002, *Solar Phys.* **210**, 3.

Mann, G., Aurass, H., Voigt, W., and Paschk, J.: 1992, in C. Mattock (ed.), *Coronal Streamers, Coronal Loops, and Coronal and Solar Wind Composition (ESA-SP348)*, ESA, Paris, p. 129.

Newkirk, G.A.: 1961, *Astrophys. J.* **133**, 983.

Pick, M., Malherbe, J.-M., Kerdraon, A., and Maia, D.: 2005, *Astrophys. J.* **631**, L97.

Scherrer, P.H., Bogart, R.S., Bush, R.I., Hoeksema, J.T., Kosovichev, A.G., Schou, J., *et al.*: 1995, *Solar Phys.* **129**, 188.

Sprangle, P. and Vlahos, L.: 1983, *Astrophys. J.* **273**, L95.

Tousey, R.: 1973, in M.J. Rycroft and S.K. Runcorn (eds.), *Space Research*, Vol. XIII, Academie-Verlag, Berlin, p. 173.

Wang, T., Yan, Y., Wang, J.L., Kurokawa, H., and Shibata, K.: 2002, *Astrophys. J.* **572**, 280.

Yan, Y.: 2005, in K. Dere, J. Wang, and Y. Yan (eds.), *Coronal and Stellar Mass Ejections*, IAU Symp. No. 226, Cambridge, p. 277.

Yan, Y., Yu, Q., and Shi, H.: 1993, in J.H. Kane, G. Maier, N. Tosaka, and S.N. Atluri (eds.), *Advance in Boundary Element Techniques*, Springer-Verlag, New York, p. 447.